Electrochemical investigation of chromium nanocarbide coated Ti-6Al-4V and Co-Cr-Mo alloy substrates

Viswanathan Swaminathan[a, b], Haitong Zeng[c], Daniel Lawrynowicz[c], Zongtao Zhang[c],

Jeremy L. Gilbert[a, b]

[a] Department of Biomedical and Chemical Engineering, Syracuse University, Syracuse, NY, USA

[b] Syracuse Biomaterial Institute, Syracuse University, Syracuse, NY, USA

[c] Stryker Orthopedics, Mahwah, NJ, USA

Corresponding author information:

Jeremy L. Gilbert, Ph.D.
Department of Biomedical and Chemical Engineering
318 Bowne Hall
Syracuse University
Syracuse, NY -13210
Phone: 315-443-2105
Email: gilbert@syr.edu

ABSTRACT:

This study investigated the electrochemical behavior of chromium nano-carbide cermet coating applied on Ti-6Al-4V and Co-Cr-Mo alloys for potential application as wear and corrosion resistant bearing surfaces. The cermet coating consisted of a highly heterogeneous combination of carbides embedded in a metal matrix. The main factors studied were the effect of substrate (Ti-6Al-4V versus Co-Cr-Mo), solution conditions (physiological versus 1M H_2O_2 of pH 2), time of immersion (1 versus 24 hours) and post coating treatments (passivation and gamma sterilization). The coatings were produced with high velocity oxygen fuel (HVOF) thermal spray technique at atmospheric conditions to a thickness of 250 µm then ground and polished to a finished thickness of 100 µm and gamma sterilized. Native Ti-6Al-4V and Co-Cr-Mo alloys were used as controls. The corrosion behavior was evaluated using potentiodynamic polarization, mechanical abrasion and electrochemical impedance spectroscopy under physiologically representative test solution conditions (Phosphate buffered saline, pH 7.4, 37˚C) as well as harsh corrosion environments (pH~2, 1M H_2O_2, T= 65˚C). Severe environmental conditions were used to assess how susceptible coatings are to conditions that derive from possible crevice-like environments, and the presence of inflammatory species like H_2O_2. SEM analysis was performed on the coating surface and cross-section. The results show that the corrosion current values of the coatings (0.4 - 4 µA/cm^2) were in a range similar to Co-Cr-Mo alloy. The heterogeneous microstructure of the coating influenced the corrosion performance. It was observed that the coating impedances for all groups decreased significantly in aggressive environments compared with neutral and also dropped over exposure time. The low frequency impedances of coatings were lower than controls. Among the coated samples, passivated nanocarbide coating on Co-Cr-Mo alloy displayed the least corrosion resistance. However, all the coated materials demonstrated higher corrosion resistance to mechanical abrasion compared to the native alloys.

Key words: Coatings, chromium carbide, biomaterials, corrosion, EIS

1. INTRODUCTION

Wear between two mating surfaces may result in oxide fracture and exposure of reactive base alloy to the corrosive media. The subsequent electrochemical events (oxidation and reduction reactions) in a restricted geometry or crevice-like environment, can lead to accelerated corrosion of the implant by the well known phenomenon of tribocorrosion, or mechanically assisted crevice corrosion [1-4]. State-of-the-art bearing surface technology typically uses metal-on-polymer, metal-on-metal, and ceramic-on-ceramic couples. Each has known advantages and disadvantages. For bulk ceramic heads on hip prostheses the risk of ceramic fracture, while reduced from early studies, remains a potential failure mode and there are recent reports of unacceptable squeaking [5, 6]. Metal bearing surfaces are limited to Co-Cr-Mo alloys since Ti alloys exhibit poor oxide wear resistance. Even with Co-Cr-Mo alloys, wear-assisted corrosion does still occur, elevating metal-ion levels in the blood [7-9].

One approach under investigation is the use of surface modification techniques such as application of hard coatings to metal substrates to improve their tribological characteristics and also reduce the incidence of wear-particle induced osteolysis [10-17]. Application of TiN coating on implant bearing surfaces is one successful surface modification approach for improvement in wear and corrosion resistance [11-13]. There are other ceramic materials such as Al_2O_3 and ZrO_2 which have proven to be beneficial in improving the wear and corrosion performance of articulating surfaces [14-17]. This excellent behavior of ceramic materials has been attributed to their better electrochemical resistance, higher abrasion resistance and better surface wettability features compared with metallic implant materials.

Chromium carbides represent a major family of interstitial carbides of group **6** metals in the periodic table. Chemical stability, corrosion resistance and high hardness are the notable properties of group **6** carbide elements. When these elements are combined with a metal matrix such as chromium both wear resistive and corrosion resistive coatings can be obtained [18]. High hardness combined with the electrochemical resistance of the carbide elements could prevent wear-related corrosion activities and enhance the load bearing capacity of native Ti-6Al-4V and Co-Cr-Mo alloys. Also, due to higher particle velocity and relatively lower flame temperature associated with HVOF spraying technique, a dense cermet coating with relatively lower porosity and less phase transformation can be achieved [19, 20].

Various techniques have been used to assess the corrosion characteristics of surfaces and coatings including polarization, abrasion and electrochemical impedance spectroscopy (EIS). Electrochemical impedance spectroscopy is a non destructive technique that has been used extensively to analyze the protective ability of coatings [21, 22]. Equivalent circuit model analysis of impedance data provides reasonable estimates of the resistive and capacitive characteristics of the interface and the coating itself which are highly influenced by the heterogeneous character of the coating and the associated conductive paths. The environments in which coatings and alloy surfaces operate in-vivo are very different from the simplified solutions used in in-vitro corrosion testing. For example, recent retrieval studies show that crevices in modular tapers can reach low pH and highly aggressive conditions sufficient to induce pitting in Ti-6Al-4V [23]. Also, if a highly inflammatory condition exists in-vivo, then byproducts of superoxides (reactive oxygen species, ROS) can be present. This includes hydrogen peroxide. Thus, the goal of this study is to investigate the corrosion behavior of Co-Cr-Mo and Ti-6Al-4V alloys surface modified by application of a thick chromium carbide cermet coating (100 μm). In this study polarization testing, abrasion electrochemical testing and, EIS were applied to investigate nanocarbide coated Co-Cr-Mo and Ti-6Al-4V alloys exposed to phosphate-buffered saline and also a more acidic environment to mimic aggressive crevice and/or surface inflammatory conditions. Changes in coating impedance over time were also explored. The effect of nanocarbide surface coatings and pre-coating treatment conditions on the electrochemical behavior of the Co-Cr-Mo and Ti-6Al-4V alloys was evaluated using cyclic potentiodynamic polarization and the degree of corrosion resistance was compared to the native Ti-6Al-4V and Co-Cr-Mo alloys based on the corrosion current density and transpassive potential values. Resistance to mechanically assisted corrosion was evaluated by a simple abrasion procedure under potentiostatic conditions [10, 24]. The specific questions to be addressed by this study are –do nanocarbide coatings improve the corrosion behavior of Co-Cr-Mo and Ti-6Al-4V surfaces? Does an aggressive environment degrade the corrosion behavior of these coatings? How does short term (24 hr) immersion affect coating corrosion resistance?

2. EXPERIMENTAL

Table 1 lists the summary of the sample materials investigated in this study. Chromium nanocarbide coatings on Co-Cr-Mo or Ti-6Al-4V femoral heads were produced with high velocity oxygen fuel (HVOF) spraying method using powders that had 75% of chromium carbide ($Cr_{23}C_6$) phase and 25% of CoCrMo alloy phase. The CoCrMo metal phase is identical to ASTM F75 CoCrMo in composition. Coatings were sprayed in normal atmospheric conditions to a thickness of 250 μm then ground and polished to a final thickness of 100 μm and a smooth mirror-like finish. Coatings were cleaned and gamma sterilized. For sample #C, coating surface treatment included nitric acid passivation prior to gamma sterilization. A Scanning Transmission

Electron Microscope image shown in Fig. 1 reveals nano-sized grains in the coating. Further details on the coating deposition process can be obtained elsewhere [25]. Coating fabrication, polishing and treatment were done at Stryker Orthopedics Inc., (Mahwah, NJ) and the finished materials were tested without any further polishing or treatments. The control group consisted of native alloy surfaces of Co-Cr-Mo alloys and Ti-6Al-4V alloys in the form of 42 mm heads of hip prostheses also obtained from Stryker. The samples were prepared for electrochemical testing by applying an acrylic insulation coating in a circle around the test region to isolate the same amount of area in each test. In calculating the area, a mathematical correction was applied to adjust for the real curvature of the head samples. Tests were repeated at least three times for all conditions evaluated.

The experimental setup for all electrochemical measurements done in this study consisted of a three electrode cell arrangement. The Potentiostat/Impedance system (Solartron 1280C, UK) was used for electrochemical testing (Polarization and EIS). An Ag/AgCl electrode was used as reference electrode and carbon rod was used as the counter electrode. Samples were rinsed with ethanol and deionised water before subjecting to any testing. Data acquisition/analysis for potentiodynamic corrosion analysis and electrochemical impedance spectroscopy (EIS) was performed using Corrware 2.0/ CorrView 2.0 and Zplot 2.0/ Zview 2.0 software (supplied by Scribner Associates), respectively.

Prior to potentiodynamic polarization, the open circuit potential (OCP) of each sample was determined for 1-hour while immersed in phosphate buffered saline (PBS) at 37˚ C. In this way the test sample was allowed to equilibrate, and the 1-hour potential was recorded as the OCP. At the end of 1-hour, coated and substrate surfaces were subjected to cyclic potentiodynamic polarization with a starting and final potential of -1 V (vs. Ag/AgCl reference electrode), vertex potential of +1 V (vs. Ag/AgCl reference electrode) and a scan rate of 1 mV/sec. Plots of potential versus log current density were constructed for each test. Only PBS at 37˚ C and pH 7.4 solution conditions were used for these tests. A very negative starting potential (-1 V) was chosen because modular interfaces associated with orthopedic devices can experience cathodic shifts much more negative than the resting OCP in the event of surface abrasion due to micro-motion and cyclic loading in-vivo. Data analysis at the end of polarization testing involved identifying the corrosion current density (i_{corr}), the zero current potential (ZCP), the transpassive potential (if any) and the presence of hysteresis (if any) associated with the reverse scan. ZCP is the potential at which the current density goes through zero (i.e., transition from cathodic to anodic currents) and can be different than OCP depending on the starting voltage. Transpassive potentials (E_t) are where the corrosion current densities rise rapidly with increasing potential and indicate loss of passive protection of the surface. In this study, since there was no evidence of any pitting in the surface, this current rise is not associated with breakdown potential. E_t was calculated from the polarization curve where the current density attained a value of 10 $\mu A/cm^2$ or higher. The corrosion current density (i_{corr}) was obtained from the polarization curve by extrapolation of the cathodic branch of the polarization curve to the ZCP. The presence of hysteresis will indicate any pitting or crevice corrosion associated with the surface. SEM analysis (JEOL 5600) using both secondary and backscattered electrons was also done prior to and after corrosion testing to evaluate the coating structure.

For abrasion measurements, the sample surfaces were potentiostatically held at 0 V (vs. Ag/AgCl), and while immersed in PBS (at room temperature) a known area of the surface was manually abraded using emory paper (600 grit) for a total period of 3 minutes. The abrasion process involved a simple rubbing action on the sample surface with a piece of emory paper.

This test did not involve any defined loading conditions during abrasion however the applied load was sufficient to induce significant electrochemical responses in both Ti-6Al-4V and Co-Cr-Mo uncoated alloys. Susceptibility to mechanically assisted corrosion was assessed with the help of current density versus time plots generated during the course of abrasion. Coated surfaces were looked under optical microscope for evidence of any coating wear-through due to abrasion.

For electrochemical impedance spectroscopy (EIS) analysis, the sample surfaces were either exposed to PBS (pH 7.4, 37 ˚C) or to a very acidic media PBS with HCl to adjust pH and H_2O_2 to obtain a 1M solution (pH 2 ± 0.5, T≈ 65-70 ˚C). Impedance was monitored at 0 hr and 24 hr for both environments. For the tests done in acidic media, the samples were stored at 37 ˚C over this 24 hour time period. Before starting the impedance measurements, sample surfaces were allowed to equilibrate for 15 minutes. Then, the samples were potentiostatically held at their OCP and a small (10 mV) sinusoidal voltage was applied to the interface, while the frequency of the input voltage was systematically varied from 20 KHz to 5 mHz. The impedance data is then obtained as a function of frequency of the applied voltage. The analysis included developing typical impedance models for coated and non-coated electrode surfaces and curve-fitting using a non-linear least squares program in ZView 2.0. The standard circuit model for non-coated surfaces (Randle's circuit) was modified to contain a constant-phase element (CPE) in place of the capacitance element to address the non-ideal behavior of the interface. CPE impedance is given by $Z= 1/ ((i\omega)^{\alpha} Q)$, where Q is a capacitance-like element, ω is the frequency, i is the imaginary number, and α is an exponent between 0 and 1(when α =1, system behaves like an ideal capacitor and when α =0, it behaves like an ideal resistor). The Randle's model applied for native Ti-6Al-4V and Co-Cr-Mo alloy surface comprised of a bulk electrolyte solution resistance (R_s), in series with a parallel combination of a constant phase element (CPE_{ox}) and resistance (R_{ox}) of the oxide. Coated surfaces were studied using both the Randle's model and a modified circuit containing CPE(CPE_{ox}) and resistance (R_{ox}) for the oxide and an embedded parallel combination of resistance(R_{coat}) and CPE(CPE_{coat}) to describe the effect of coating (see Fig. 2). The modified circuit will give rise to a two-peak phase angle response due to the presences of a second set of electrode components that account for the coating's presence.

Statistical analysis of the data included performing one-way ANOVA and Tukey post-hoc test using SPSS 16.0 statistical analysis software. Sample groups were compared based on the polarization and impedance electrochemical parameters. The effect of immersion time on the impedance behavior of individual sample groups was also analyzed. We used a p-level of 0.05 for all statistical tests.

3. RESULTS

3.1 Polarization measurements

The mean open-circuit potential values of the coated and non-coated alloys at the end of 1hr are summarized in Table 2. At the end of 1 hr immersion in PBS, the mean open circuit potential of all the coated samples were in the range of 0 to -100 mV (vs. Ag/AgCl), similar to the range seen for native Co-Cr-Mo alloy. Also shown in Table 2 are the mean ± SD values of the zero current potential (ZCP), transpassive potential (E_t) and corrosion current density (i_{corr}) for each of the control group and test group materials determined from the polarization curves shown in Fig. 3. The mean ± SD values for native Ti-6Al-4V and Co-Cr-Mo alloys was previously reported [10]. In general, the zero current potentials of all the materials tested are lower than their respective open circuit potential due to application of highly reducing initial potential (-1 V vs. Ag/AgCl) during the polarization measurements. No statistically significant differences were observed among any of the samples in terms of E_{ocp} ($p > 0.05$). The ZCP value of sample #C and Co-Cr-Mo alloy was significantly lower than that of the other samples tested in this study ($p < 0.025$).

The corrosion current density value for Ti-6Al-4V alloy and Co-Cr-Mo obtained from cathodic extrapolation of the polarization curves was found to be 0.25 µA/cm^2 and 6 µA/cm^2, respectively. The corrosion response of these alloys was typical of passivating alloys. A significant passive current density region was observed for Co-Cr-Mo alloy in the potential range of -400 mV to + 400 mV. For Ti-6Al-4V alloy, +400 mV and higher marked the constant passive current density region. Among the control group, Co-Cr-Mo alloy reached the transpassive current density (10 µA/cm^2) at about +500 mV, however, for Ti-6Al-4Valloy, the current density value did not reach the transpassive value at the end of the forward scan.

Among the coated samples, a significant variation in corrosion behavior across potentials was observed for different coating treatment conditions (Fig. 3). Passivated and gamma sterilized nanocarbide on Co-Cr-Mo (Sample #C) reported highest corrosion current density value (4 µA/cm^2) and lowest transpassive potential value (+ 198 mV) among the coated samples tested in this study. The transpassive potential for sample #C was significantly lower than that of the other samples tested in this study ($p < 0.001$) (see Table 2). Above the ZCP, a sharp increase in current density was observed for this sample, and in the range of potentials -200 mV to + 600 mV the electrochemical behavior appears distinctly different from the other coated samples (sample # A and # B). However, the corrosion current densities of all the coated samples are in the range of corrosion current density seen for the non-coated Co-Cr-Mo alloy. Also, the transpassive potential of the coated alloys except for sample #C are more positive (above + 500 mV) and comparable to Co-Cr-Mo alloy response. The shape of the polarization curves of the coated alloys above the transpassive potential was very similar to Co-Cr-Mo alloy behavior. None of the samples exhibited any hysteresis during the reverse scan. The corrosion current (i_{corr}) for native Ti-6Al-4V alloy was significantly lower than that of native Co-Cr-Mo alloy ($p < 0.05$). No significant differences were observed between the coated samples or between the coated and native alloy surfaces.

The backscattered SEM micrographs of Fig. 4 reveal the heterogeneous nature of the nanocarbide coating surface (Fig. 4a) and cross-section (Fig. 4b), which is typical of thermal spray process. The chemical heterogeneity due to different phases may influence the corrosion behavior of the overall surface. The brighter regions in the micrograph are the metallic phase which forms a heterogeneous network filled with dark carbide phases of various shapes.

3.2 Abrasion measurements

The results of the potentiostatic abrasion tests on a nanocarbide coated Co-Cr-Mo alloy (sample #A) and non-coated Co-Cr-Mo alloy are shown in Fig. 5. For both coated and non-coated alloys the current densities increased during abrasion and when abrasion was stopped the current densities recovered back to the rest level. However, from the figure, the abrasion current density values of the chromium nanocarbide coating were at least an order of magnitude lower than that of the native oxide surface. The abrasion response of the samples #B and #C was similar to that seen for sample #A. Also, abrasion did not cause any wear-through of the coatings.

3.3 Electrochemical impedance spectroscopy measurements

The results of EIS measurements are represented as Bode plots. The impedance response of the coated and non-coated alloys obtained at the end of 1 hour in PBS (pH 7.4) at 37 ˚C is shown in Fig. 6. From Fig. 6a, the impedance versus frequency plots of Ti-6Al-4V alloy and Co-Cr-Mo alloy show a highly capacitive behavior, typical of the passivating alloys where the coatings show reduced low frequency impedances. The near ideal capacitive character of Ti-6Al-4V alloy and Co-Cr-Mo alloy is also indicated in the phase angle plot (Fig. 6b) by a broad single peak response with the phase angle close to -90˚ over a frequency range of 100 – 0.1 Hz.

From Fig. 6a, among the coatings, sample #C recorded the lowest low frequency impedance (35 KΩ-cm^2) and sample #A recorded the highest low frequency impedance (150 KΩ-cm^2). As seen from the phase angle plot of Fig. 6b, the coated surfaces exhibited lower phase angles and more of a double peak behavior typical of coatings. The two peaks were close to each other and appeared in the frequency range of 0.1 Hz to 1000 Hz. The high frequency peak is brought out by the electrochemical interaction at the coating/solution interface and low frequency peak is brought out by the electrochemical interaction at the coating/substrate interface [21].

The one-hour impedance response of the coated and non-coated alloys obtained during exposure in a more aggressive condition (pH ≈ 2 at T ≈ 65 ˚C) with H_2O_2 is shown in Fig. 7. The impedance plot (Fig. 7a) shows more than two orders of magnitude drop in the low frequency impedance for Ti-6Al-4V alloy and an order of magnitude drop for Co-Cr-Mo alloy. Also, a narrow single peak phase angle (Fig. 7b) response was observed for both Ti-6Al-4V alloy and Co-Cr-Mo alloy, indicating that the near ideal capacitive nature of the oxide surfaces is diminished in aggressive conditions. For the coated alloys, the low frequency impedances were in the range seen for the native alloys (about 5 KΩ-cm^2, from Fig. 7a). The phase angle response of the coatings was more like an active surface with a distinct single peak appearing in the frequency range of 1 Hz to 1000 Hz (Fig. 7b).

Fig. 8 and Fig. 9 are representative Bode plots of the effect of exposure time on the impedance behavior of non-coated (Co-Cr-Mo) alloy and coated (sample #A) alloy, respectively.

From the impedance plots of Fig. 8a and 9a it is apparent that irrespective of the solution conditions, the impedances of both the coated and non-coated alloys dropped over time in the mid- frequency range. Also, from the phase angle plots of Fig. 8b and Fig. 9b, it appears that over time the phase angle peak becomes narrower and shifts towards higher frequencies.

A summary of the ac circuit model parameters obtained by non–linear least square fitting of the impedance data using ZView 2.0 impedance analysis software is presented for neutral and acidic environment in Table 3 and Table 4 respectively. Note that the values are denoted as mean ± SD for n = 3. The impedance parameter values for both solution environments show high variability as indicated by the standard deviation values. For the coated surfaces some of this variability can be attributed to the overall heterogeneity of the coating.

For exposure in PBS (Table 3), the non-coated and coated surfaces were modeled using the circuits shown in Fig. 2. For the coated alloys, the outer part of the embedded configuration (R_{coat} and CPE_{coat}) explains the high frequency response of any coated material, where CPE_{coat} is associated with the high frequency peak in the phase angle plot. The inner part of the embedded configuration (R_{ox} and CPE_{ox}) explains the low frequency response of any coated material, where CPE_{ox} is associated with the low frequency peak in the phase angle plot. From Table 3, the mean solution resistance (R_s) for the native surfaces in PBS were higher than the coated surfaces, in the range of 20 -24 Ω-cm^2 and it decreased with time. The oxide layer capacitance (CPE_{ox}) of the native surfaces was about 25 (μF/cm^2) (rad/s)$^{1-\alpha}$. The exponent values (α) closer to 1 indicates near capacitive behavior of these alloys. The resistance (R_{ox}) of the native oxide surfaces was very high, in the range of mega ohms which implies a high corrosion resistance. The values of both R_{ox} and CPE_{ox} increased with time.

For the nano-carbide coated surfaces in PBS, the R_{coat} value was very low (2 KΩ-cm^2- 4

KΩ-cm^2) and the CPE$_{coat}$ value was in the range of (26 -158 µF/cm^2) (rad/s)$^{1-\alpha}$ with sample #C reporting the highest CPE$_{coat}$ value (from Table 3). The exponent value of the CPE$_{coat}$ indicated higher heterogeneity associated with the surface and for sample #C the exponent value was significantly lower ($p < 0.05$) from that of sample #A and sample #B. The interfacial capacitance (CPE$_{ox}$) and resistance (R$_{ox}$) values were on par with the native surfaces except for sample #C which reported high CPE$_{ox}$ and very low R$_{ox}$ value (from Table 3). The coating circuit model also suggested higher heterogeneity ($\alpha < 0.8$, from Table 3) associated with the coating/substrate interfacial layer (CPE$_{ox}$) compared to the native oxides. With time the CPE$_{coat}$ and CPE$_{ox}$ values for the coated samples increased whereas the R$_{coat}$ and R$_{ox}$ values decreased or increased slightly (from Table 3). At 24 hr time point, the α value associated with CPE$_{coat}$ for sample #C was significantly lower ($p < 0.025$) than sample #A. Also, α value associated with CPE$_{coat}$ for sample #B significantly decreased with time ($p < 0.01$). No significant differences ($p > 0.05$) were observed among any of the samples in terms of other circuit parameters.

Under aggressive exposure conditions only single peak phase angle response was observed for the coated surfaces (see Fig. 7b). Therefore, both coated and non-coated surface impedance response was modeled using a Randle's circuit containing a CPE element as shown in Fig. 2 (left). From Table 4, for exposure in aggressive environment, the mean R$_s$ value of all the surfaces ranged from 9 – 13 Ω-cm^2 and the mean R$_{ox}$ values were very low, in the range of kilo ohms (4 - 20 KΩ-cm^2). The capacitance values of both the coated and non-coated surfaces were relatively higher (34- 105 (µF/cm^2) (rad/s)$^{1-\alpha}$) than those obtained with the PBS. In general, the values of R$_s$ and R$_{ox}$ decreased with time and CPE$_{ox}$ increased with time. Also, from Table 4, the capacitance values (CPE$_{ox}$) for the coatings were relatively higher than that seen for the native surfaces, with higher degree of imperfection as suggested by the exponent values ($\alpha < 0.8$).

During early time, the α value associated with CPE_{ox} for sample #C was significantly lower ($p < 0.05$) than that of the native surfaces. From Table 4, at 24 hr time point, the α value of all the coated surfaces was significantly lower ($p < 0.05$) than that of the native Co-Cr-Mo alloy. The effect of immersion time on the coating impedance behavior in acidic solution conditions was non-significant ($p > 0.05$).

4. DISCUSSION

The main findings of this study are that nanocarbide cermet coating, while providing a high hardness to the surface is also susceptible to electrochemical processes. These coatings corrode similarly to Co-Cr-Mo alloy. Secondly, it was found that the presence of H_2O_2 at high temperature and low pH conditions lowers the corrosion resistance of all materials. Thirdly, it appears that severe abrasion increases coatings' corrosion rate but less than that seen for native Co-Cr-Mo alloy surfaces.

From the polarization results (see Fig. 3) it is apparent that the coated surfaces are susceptible to electrochemical activity regardless of the substrate or the post-deposition treatment conditions. The coating appears to be actively involved in the charge transfer process leading to increasing current density values over the range of potential tested. This behavior of the coating is thought to be the outcome of the coating microstructure (see Fig. 4). The microstructure of a thermally sprayed coating is generally inhomogeneous and is associated with inter-particle voids and gaps [26]. Porous coating obtained by another thermal spraying method, plasma spraying, may cause accelerated corrosion of the substrate due to acidification caused in a local environment [27]. The heterogeneous microstructure of the nanocarbide coatings with the presence of small amounts of porosity within the coatings may serve as the pathways for fluid ingress and the possibility for a localized electrochemical attack. Though application of thick coatings (≥100 μm) minimize the effect of porosity associated with thermal spraying, generation of residual stresses during coating deposition may lead to formation of cracks between different layers of the coating and thereby reduce the resistance of the coating to electrolyte penetration [28]. One other possible reason contributing to the observed electrochemical behavior could be the preferential corrosion of metallic Co-Cr-Mo alloy present as the coating matrix. This is evident from the shape of the polarization curves of the coated surfaces being similar to the native Co-Cr-Mo alloy above the transpassive potential. This also explains the limited passivity of the nanocarbide coated Ti-6Al-4V surface (sample #B) compared to the native Ti-6Al-4V alloy (Fig. 3). The presence of a thick nanocarbide coating prevented the substrate titanium alloy surface from interacting with the electrolyte and the observed response is due to the coating electrochemical activity only.

It should be noted that sustained cathodic bias of the passivating alloys can alter the chemistry, valence state and thickness of the oxide film, and hence alter the electrochemical response of the surface. A very negative starting potential used in this study may have partially reduced the surface oxides of the native alloys, leading to negative shift in the ZCP compared to OCP. Electrochemical history may have altered electrochemical response of the coated surfaces as well, causing negative shift in ZCP. The substrate does not appear to play a significant role in the corrosion behavior of any of the coated surfaces because the presence of a thicker coating (100 μm) lead to a better resistance against the electrolyte. Also, absence of hysteresis in the polarization curve implies no pitting-like attack developed as a result of testing.

Among the coatings, higher current values and absence of any significant current limiting region for sample #C suggests that this surface is more electrochemically active than sample #A and sample #B. Although passivation treatments are thought to enhance corrosion resistance of the surface some studies on titanium alloy surface passivation have reported otherwise [29-31]. In our study, post-deposition nitric acid treatment could have altered the coating (sample #C) such as to negatively impact the corrosion resistance of the surface. Also, during polarization testing highly reducing initial electrochemical conditions may have resulted in partial reduction of oxide film formed by the passivation treatment on sample #C leading to exposure of a highly heterogeneous coating microstructure to the solution. There are other surface controlled factors such as roughness that could impact the observed corrosion response. One of the limitations in this study is that roughness was not characterized at the individual test areas before and after corrosion testing. Based on the current density values and transpassive potential (E_t) values (Table 2) obtained from the polarization testing, sample #C can be considered the least corrosion resistant among the coated samples.

Susceptibility to mechanically assisted corrosion of the coating was assessed by mechanically disturbing the surface and seeing whether the electrochemical stability of the surface is altered or not. Severe abrasion was done using an emory paper to abrade the surface, and this hand abrasion method could have introduced variability in the loading. In general, for all coated surfaces tested in this study, larger difference between the abrasion currents and at-rest currents indicated that electrochemical stability of the coating was altered due to the abrasion process, and the measured currents are due to dissolution of metal ions in to the solution. The results clearly indicate that the nanocarbide cermet coatings could reduce mechanically assisted corrosion activities associated with native alloy surfaces.

For impedance testing, both normal PBS and a severe corrosion environment containing H_2O_2 were investigated. The rationale for testing in a harsh solution is that it provides a low pH, high oxidizing and high temperature conditions that represents an extreme in solution conditions.

It is known for example, that hydrogen peroxide arises during inflammation and temperature and pH shifts are possible in-vivo in crevice-like geometries undergoing wear. While this solution may be extreme, it does show that these materials do alter their behavior as solution conditions become more aggressive.

Higher impedance values and broad single peak phase angle response of the native alloys exposed to PBS implies high corrosion resistance of these surfaces. Immersion time did not have much of an effect on the impedance response of the native alloys, indicating that a highly stable oxide layer was formed on these surfaces. However, during exposure to high temperature, acidic media, H_2O_2 solution the phase angles shifted and the impedance values dropped significantly, indicating low corrosion resistance of the native surfaces in this environment. This is also evident from the model parameter values for the native oxide surfaces (from Table 4). For Ti-6Al-4V alloy surface the presence of H_2O_2 must have caused increased oxidation of the titanium, leading to a less dense and more defective oxide structure [32]. With time, the impedance values of the native surfaces dropped further indicating that the corrosion resistance of these surfaces is deteriorating rapidly in this environment.

Impedance behavior of the coatings in PBS was very different from the native oxides as is expected from a coated surface. The coating behaves more like a conductive element rather than a dielectric material due to the influence of microstructure on the capacitive aspects of the coating and the presence of metal phase in the coating. Immersion time had some effect on the coating impedance behavior. The surface initially presented to the solution transformed to a more active, less passive surface over 24 hours. Among the coatings, based on the impedance results, sample #C can be considered least corrosion resistant. The corrosion resistance of sample #A and sample #B were similar to native oxide surfaces.

The impedance response of the coated surfaces exposed to acidic conditions implies that under severe corrosive environment conditions the coated surface behaves just like the underlying surface, which in our study is native Ti-6Al-4V and native Co-Cr-Mo alloy. The presence of highly acidic environment in contact with a highly heterogeneous metal-cermet surface may have caused severe electrochemical attack on the coated surfaces. From the model parameter values shown in Table 4, the corrosion resistance of the coated surfaces is comparable to the native Co-Cr-Mo alloy. Again, as with the case of PBS, the capacitance increased over time, implying that the capacitance generating layer is becoming less dense with time.

When new coating materials are being developed such as the nanocarbide coatings considered in this study, it is important to understand their basic electrochemical behavior along with their wear performance. Therefore, experiments were designed with the electrochemical view point to answer certain fundamental questions which will enable us to draw conclusions on the suitability of this particular coating material for application in bearing materials. The nanocarbide cermet coating considered in this study has suitable electrochemical characteristics for bearing applications; however, further testing has to be done to characterize the wear performance of the coating before drawing any conclusions on the potential use as a bearing material. Also, results from this study show that the electrochemical behavior of the coated surfaces is strongly influenced by the coating microstructure and coating treatment conditions.

Several studies on corrosion behavior of the coated surfaces have reported the influence of coating microstructure on the corrosion performance. In a study by Reclaru et al, Ti-coated Co-Cr-Mo alloy surfaces showed inferior corrosion resistance even with a thick coating (250 µm to 1000 µm) due to porous coating morphology [27]. In another study, the influence of post-deposition heat treatment on the corrosion behavior of 450 µm thick Cr_3C_2-NiCr coating vacuum plasma sprayed on steel was evaluated. Significant improvement in the corrosion resistance of post-heat treated coating was attributed to the microstructural changes that decreased the interconnected porosity and increased the adhesion of the coating to the substrate [33].

Coating microstructure is related to thermal spray parameters such as spray temperature, time, and impact velocity. Therefore, optimization of these parameters and conditioning treatments could further enhance the electrochemical performance of the coatings.

5. CONCLUSIONS

This study has reported on the electrochemical behavior of high velocity oxygen fuel (HVOF) thermal sprayed nanocarbide cermet coatings applied to Co-Cr-Mo and Ti-6Al-4V substrates. It was found that polarization behavior of the coated surfaces in pH 7.4, 37˚C PBS is comparable to native Co-Cr-Mo alloy. Abrasion results show that chromium carbide coatings are susceptible to mechanically assisted corrosion but less than seen with native Co-Cr-Mo surfaces. The impedance of the newly developed coatings was similar to the native oxide surfaces when exposed to PBS. The more severe environment significantly decreased the corrosion resistance of these surfaces with acidic peroxide solutions increasing the rate of corrosion. Coating treatment conditions did affect the electrochemical behavior of the coatings, with passivated coating (sample #C) demonstrating least corrosion resistance among the coated samples. Immersion time lowered the coating impedance in both PBS and acidic environment conditions. Overall, the nanocarbide cermet coatings considered in this study has suitable electrochemical characteristics for further consideration and assessment as a bearing surface.

Acknowledgements

This work was supported by Stryker Orthopedics Inc. Mahwah, NJ, USA

References

[1] J.L. Gilbert, J.J. Jacobs, The mechanical and electrochemical processes associated with taper fretting crevice corrosion: a review, in: D.E. Marlowe, J.E. Parr, M.B. Mayor (Eds.), Modularity of Orthopedic Implants, ASTM STP 1301, American Society for Testing and Materials, Philadelphia, PA, 1997, p. 45.

[2] S.A. Brown, C.A. Flemming, J.S. Kawalec, H.E. Placko, C. Vassaux, K. Merritt, et al., Fretting corrosion accelerates crevice corrosion of modular hip tapers, J. Appl. Biomater. 6 (1995) 19.

[3] J.R. Goldberg, C.A. Buckley, J.J. Jacobs, J.L. Gilbert, Corrosion testing of modular hip implants, in: D.E. Marlowe, J.E. Parr, M.B. Mayor (Eds.), Modularity of Ortho-pedic Implants, ASTM STP 1301, American Society for Testing and Materials, Philadelphia, PA, 1997, p. 157.

[4] J.L. Gilbert, C.A. Buckley, J.J. Jacobs, In vivo corrosion of modular hip pros-thesis components in mixed and similar metal combinations. The effect of crevice, stress, motion, and alloy coupling, J. Biomed. Mater. Res. 27 (1993) 1533.

[5] J.C. Keurentjes, R.M. Kuipers, D.J. Wever, B.W. Schreurs, High incidence of squeaking in THAs with alumina ceramic-on-ceramic bearings, Clin. Orthop. Relat. Res. 466 (2008) 1438.

[6] C. Restrepo, J. Parvizi, S.M. Kurtz, P.F. Sharkey, W.J. Hozack, R.H. Rothman, The noisy ceramic hip: is component malpositioning the cause? J. Arthroplasty 23 (2008) 643.

[7] J.J. Jacobs, R.M. Urban, J.L. Gilbert, A.K. Skipor, J. Black, M. Jasty, et al., Local and distant products from modularity, Clin. Orthop. Relat. Res. 319 (1995) 94.

[8] R.M. Urban, J.J. Jacobs, J.L. Gilbert, J.O. Galante, Migration of corrosion prod-ucts from modular hip prostheses. Particle microanalysis and histopathological findings, J. Bone Joint Surg. Am. 76 (1994) 1345.

[9] R.M. Urban, J.J. Jacobs, J.L. Gilbert, S.B. Rice, M. Jasty, C.R. Bragdon, J.O. Galante, Characterization of solid produc ts of corrosion generated by modular-head femoral stems of different designs and materials, in: D.E. Marlowe, J.E. Parr, M.B. Mayor (Eds.), Modularity of Orthopedic Implants, ASTM STP 1301, American Society for Testing and Materials, Philadelphia, PA, 1997, p. 33.

[10] V. Swaminathan, H. Zeng, D. Lawrynowicz, Z. Zhang, J.L. Gilbert, Electrochem-ical investigation of chromium oxide-coated Ti–6Al–4V and Co–Cr–Mo alloy substrates, J. Biomed. Mater. Res. B: Appl. Biomater. 98B (2) (2011) 369.

[11] U. Türkan, O. Öztürk, A.E. Ero˘glu, Metal ion release from TiN coated CoCrMo orthopedic implant material, Surf. Coat. Technol. 200 (2006) 5020.

[12] A.F. Yetim, A. Alsaran, I. Efeoglu, A. C¸ elik, A comparative study: the effect of surface treatments on the tribological properties of Ti–6Al–4V alloy, Surf. Coat. Technol. 202 (2008) 2428.

[13] A. Vadiraj, M. Kamaraj, Effect of surface treatments on fretting fatigue damage of biomedical titanium alloys, Tribol. Int. 40 (2007) 82.

[14] S.K. Yen, S.W. Hsu, Electrolytic A12O3 coating on Co–Cr–Mo implant alloys of hip prosthesis, J. Biomed. Mater. Res. 54 (2001) 412.

[15] P. Kumar, M. Oka, K. Ikeuchi, K. Shimizu, T. Yamamuro, H. Okumura, et al., Low wear rate of UHMWPE against zirconia ceramic (Y-PSZ) in comparison to alumina ceramic and SUS 316L alloy, J. Biomed. Mater. Res. 25 (1991) 813.

[16] B. Cales, Y. Stefani, E. Lilley, Long-term in vivo and in vitro aging of a zirconia ceramic used in orthopaedy, J. Biomed. Mater. Res. 28 (1994) 619.

[17] M. Semlitsch, H.G. Willert, Clinical wear behaviour of ultra-high molecular weight polyethylene cups paired with metal and ceramic ball heads in com-parison to metal-on-metal pairings of hip joint replacements, Proc. Inst. Mech. Eng. H 211 (1997) 73.

[18] D. Toma, W. Brandl, G. Marginean, Wear and corrosion behaviour of thermally sprayed cermet coatings, Surf. Coat. Technol. 138 (2001) 149.

[19] P.H. Suegama, N. Espallargas, J.M. Guilemany, J. Fernández, A.V. Benedetti, Electrochemical and structural characterization of heat-treated CrC–NiCr coatings, J. Electrochem. Soc. 153 (2006) B434.

[20] V.V. Sobolev, J.M. Guilemany, J. Nutting, High Velocity Oxy-Fuel Spraying. Theory, Structure-Properties Relationships and Applications, Maney for the Institute of Materials, Minerals and Mining, London, 2004.

[21] C. Zhong, X. Tang, Y.F. Cheng, Corrosion of steel under the defected coating stud-ied by localized electrochemical impedance spectroscopy, Electrochim. Acta 53 (2008) 4740.

[22] Y. Chang, D. Wang, Corrosion behavior of CrN coatings enhanced by niobium ion implantation, Surf. Coat. Technol. 188–189 (2004) 478.

[23] D. Rodrigues, R. Urban, J. Jacobs, J. Gilbert, In vivo severe corrosion and hydro-gen embrittlement of retrieved modular body titanium alloy hip-implants, J. Biomed. Mater. Res. B: Appl. Biomater. 88 (2009) 206.

[24] J.L. Gilbert, B. Lam, Medical Device Materials V, Proceedings of Materials and Processes for Medical Devices Conference, Minneapolis, Minnesota, USA, 10–12 August 2009, 2009, p. 30.

[25] D.E. Lawrynowicz, A. Wang, E. Jones, High velocity spray technique for medical implant components, 07/11/2007; EP20070100149.

[26] V.V. Sobolev, J.M. Guilemany, Formation of splats during thermal spraying of composite powder particles, Mater. Lett. 42 (2000) 46.

[27] L. Reclaru, P.Y. Eschler, R. Lerf, A. Blatter, Electrochemical corrosion and metal ion release from Co–Cr–Mo prosthesis with titanium plasma spray coating, Biomaterials 26 (2005) 4747.

[28] J.M. Guilemany, Effects of thickness coating on the electrochemical behaviour of thermal spray Cr3C2–NiCr coatings, Surf. Coat. Technol. 153 (2002) 107.

[29] W.A. Badawy, F.M. Al-kharafi, Stability of titanium and zirconium anodic films in nitric acid solutions: EIS comparative investigation, Bull. Electrochem. 12 (1996) 505.

[30] M. Browne, P.J. Gregson, Effect of mechanical surface pretreatment on metal ion release, Biomaterials 21 (2000) 385.

[31] B.W. Callen, B.F. Lowenberg, S. Lugowski, R.N.S. Sodhi, J.E. Davies, Nitric acid passivation of Ti6A14V reduces thickness of surface oxide layer and increases trace element release, J. Biomed. Mater. Res. 29 (1995) 279.

[32] J. Pan, D. Thierry, C. Leygraf, Electrochemical impedance spectroscopy study of the passive oxide film on titanium for implant application, Electrochim. Acta 41 (1996) 1143.

[33] M. Suarez, S. Bellayer, M. Traisnel, W. Gonzalez, D. Chicot, J. Lesage, et al., Corrosion behavior of Cr3C2–NiCr vacuum plasma sprayed coatings, Surf. Coat. Technol. 202 (2008) 4566.

Figure captions

Figure 1: A transmission electron microscope image showing the size distribution of the chromium carbide cermets.

Figure 2: Models used for analysis of the impedance data for non-coated (left) and coated surfaces (right). Left: Randle's circuit for an electrode interface with a constant phase element. Right: typical impedance model for coated electrode surface containing additional set of electrode components (Rcoat and CPEcoat).

Figure 3: Representative potential versus log current density plots for each group tested in phosphate buffered saline (PBS). Note: Reverse scan is not shown for clarity. No hysteresis was observed in any of the tests.

Figure 4: SEM micrographs of untested nanocarbide coating on Co-Cr-Mo alloy (sample #A) (a) surface and (b) cross section. Images indicate highly heterogeneous microstructure of nanocarbide coating.

Figure 5: Plot of current density versus time comparing the abrasion response of a nanocarbide coating (#A) with non-coated Co-Cr-Mo alloy. Note the variation in the current density response of the surface due to abrasion and the difference in magnitude of the current density response of the coating and the native oxide surface.

Figure 6: Bode plots for Cr-carbide coated and non-coated alloys exposed in the PBS solution (pH 7.4) at 37˚C at the end of 1 hr immersion period. (a) Impedance plot (b) phase angle plot

Figure 7: Bode plots for Cr-carbide coated and non-coated alloys exposed in the acidic high temperature H_2O_2 solution (pH 2) at the end of 1 hr immersion period. (a) Impedance plot (b) phase angle plot

Figure 8: Bode plots for Co-Cr-Mo alloy exposed in neutral and acidic solution at different exposure times. (a) Impedance plot (b) Phase angle plot

Figure 9: Bode plots for Cr-carbide coated (sample #A) exposed in neutral and acidic solution at different exposure times. (a) Impedance plot (b) Phase angle plot

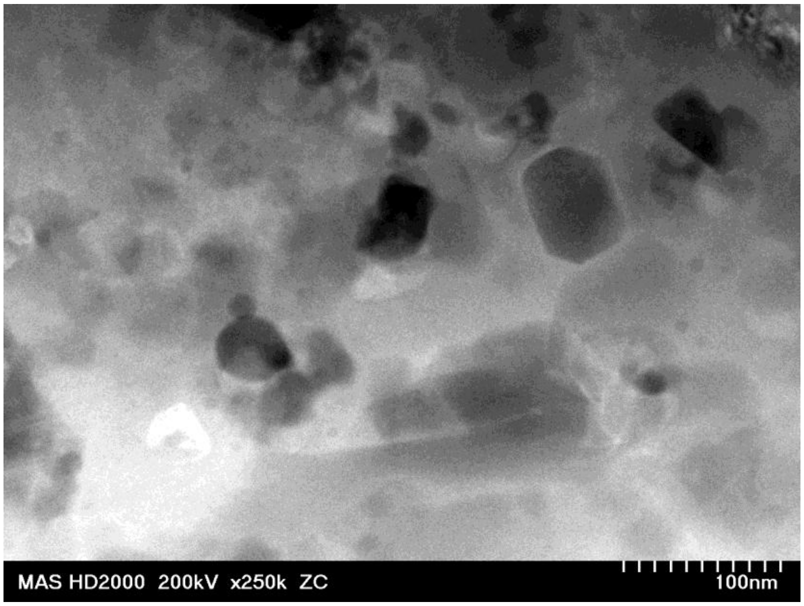

Figure 1: A transmission electron microscope image showing the size distribution of the chromium carbide cermets

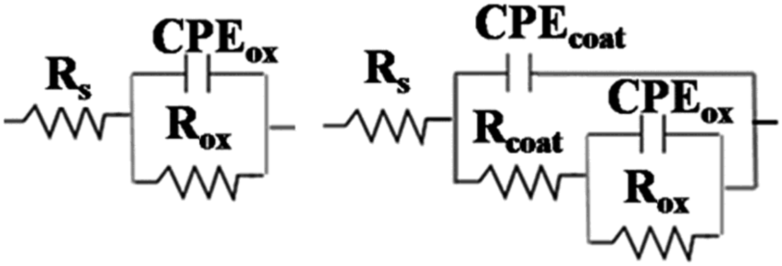

Figure 2: Models used for analysis of the impedance data for non-coated (left) and coated surfaces (right). Left: Randle's circuit for an electrode interface with a constant phase element. Right: typical impedance model for coated electrode surface containing additional set of electrode components (R_{coat} and CPE_{coat}).

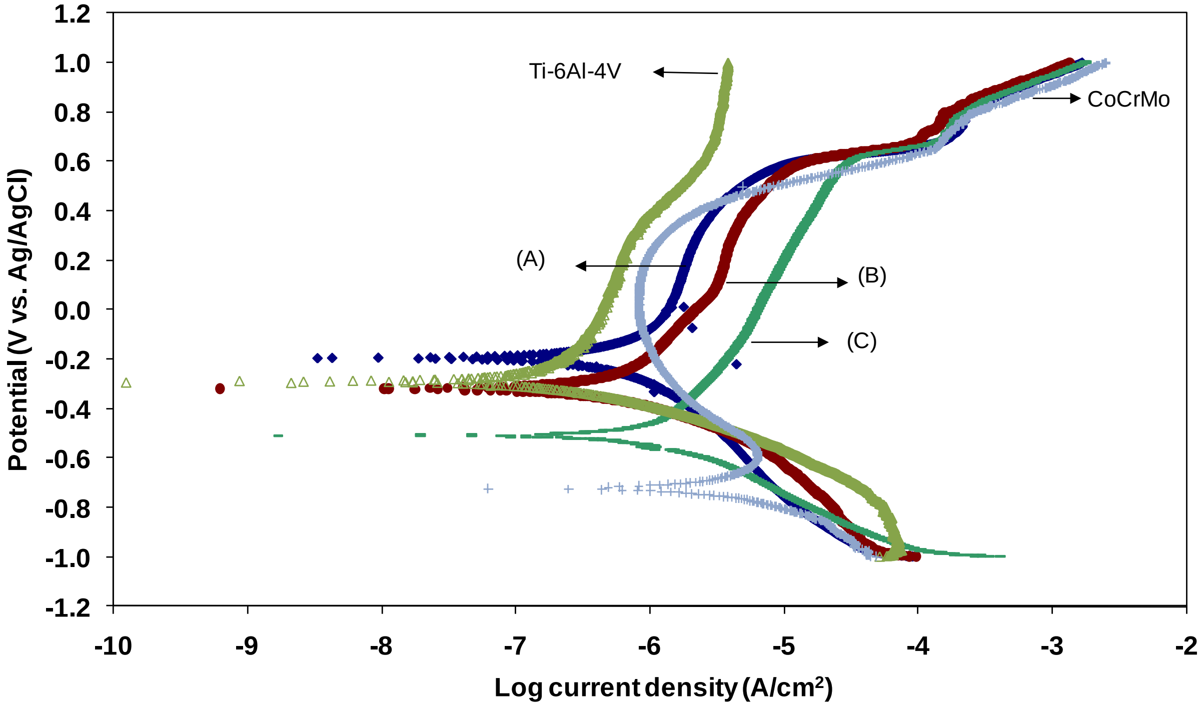

Figure 3: Representative potential versus log current density plots for each group tested in phosphate buffered saline (PBS). Note: Reverse scan is not shown for clarity. No hysteresis was observed in any of the tests.

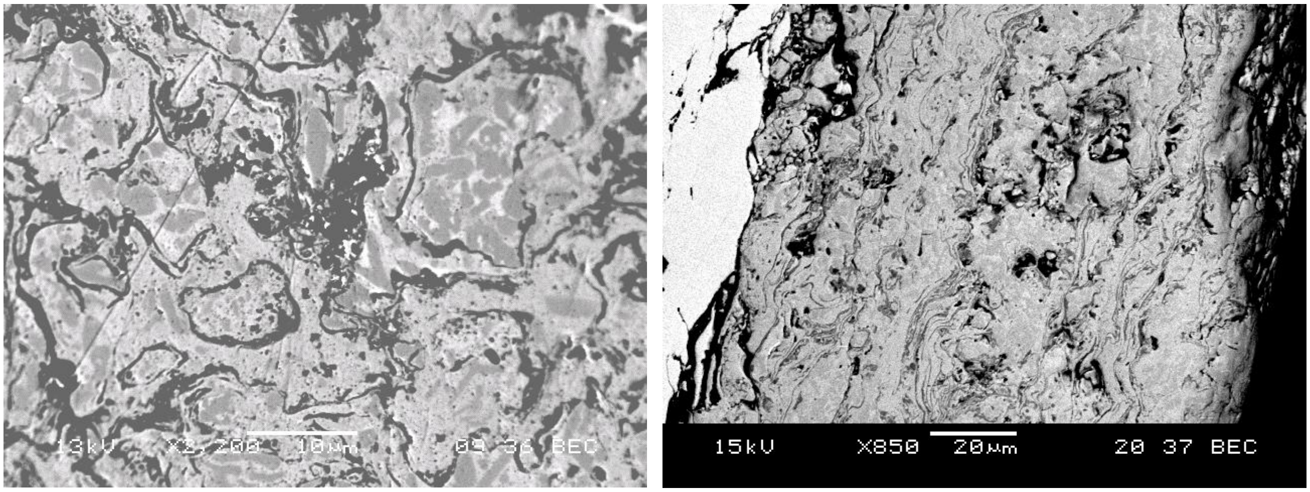

(a)

(b)

Figure 4: SEM micrographs of untested nanocarbide coating on Co-Cr-Mo alloy (sample #A) (a) surface and (b) cross section. Images indicate highly heterogeneous microstructure of nanocarbide coating.

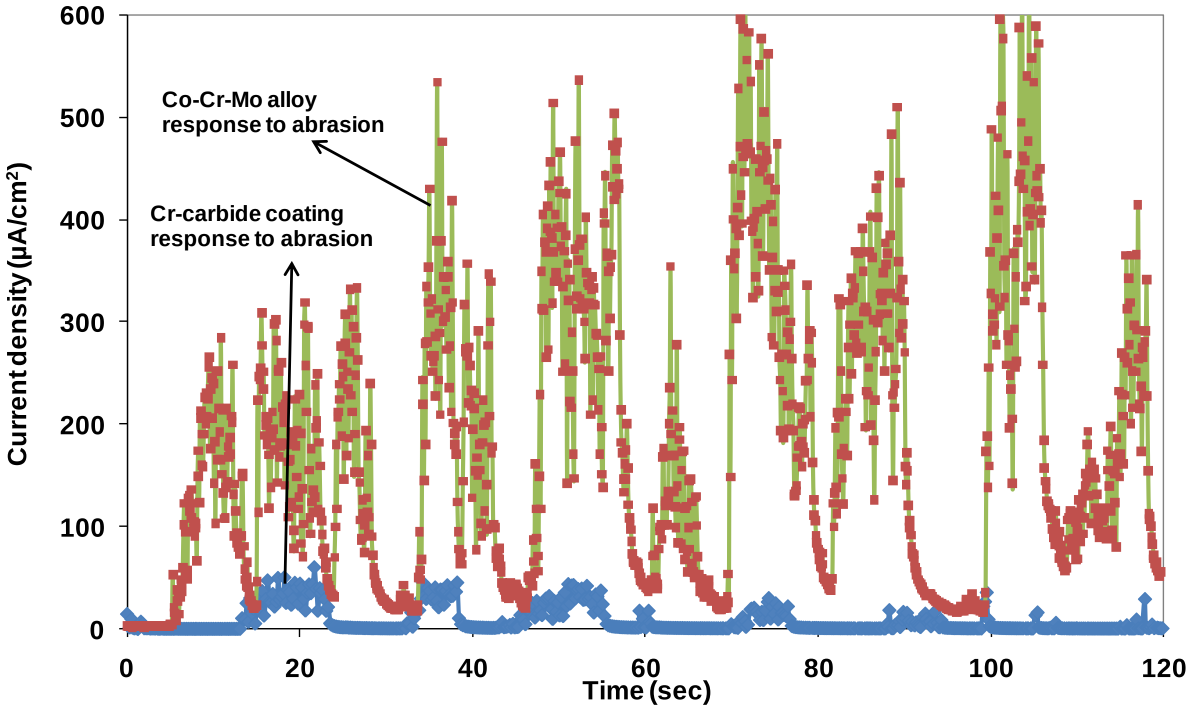

Figure 5: Plot of current density versus time comparing the abrasion response of a nanocarbide coating (#A) with non-coated Co-Cr-Mo alloy. Note the variation in the current density response of the surface due to abrasion and the difference in magnitude of the current density response of the coating and the native oxide surface.

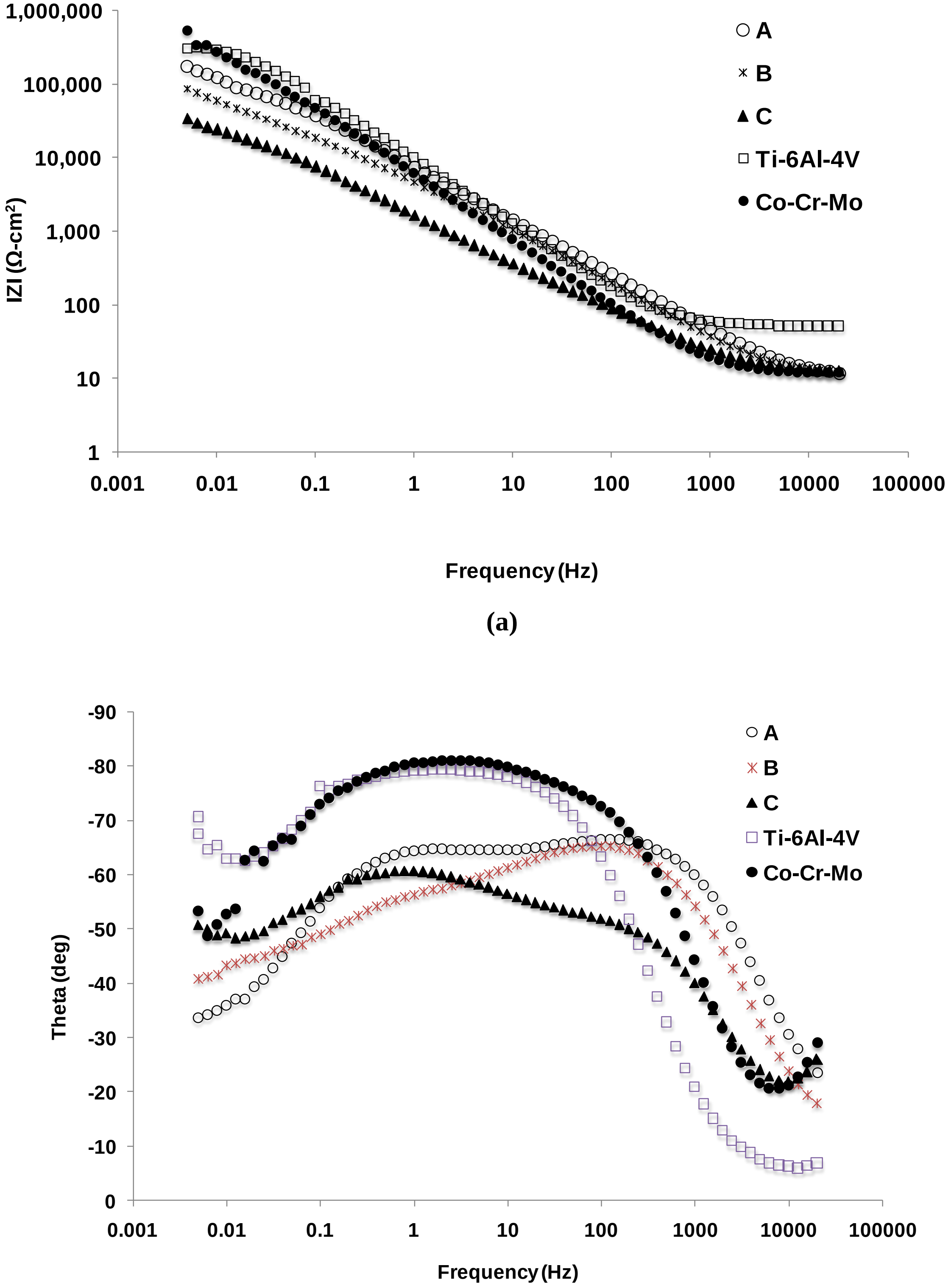

(a)

(b)

Figure 6: Bode plots for Cr-carbide coated and non-coated alloys exposed in the PBS solution (pH 7.4) at 37˚C at the end of 1 hr immersion period. (a) Impedance plot (b) phase angle plot

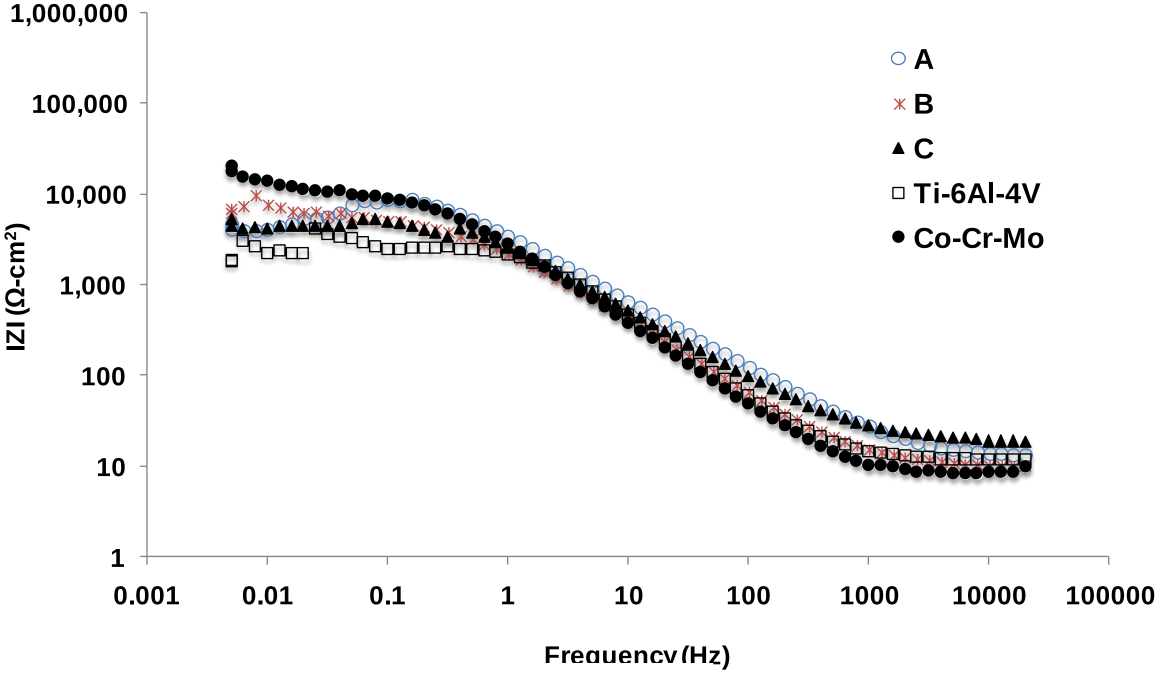

(a)

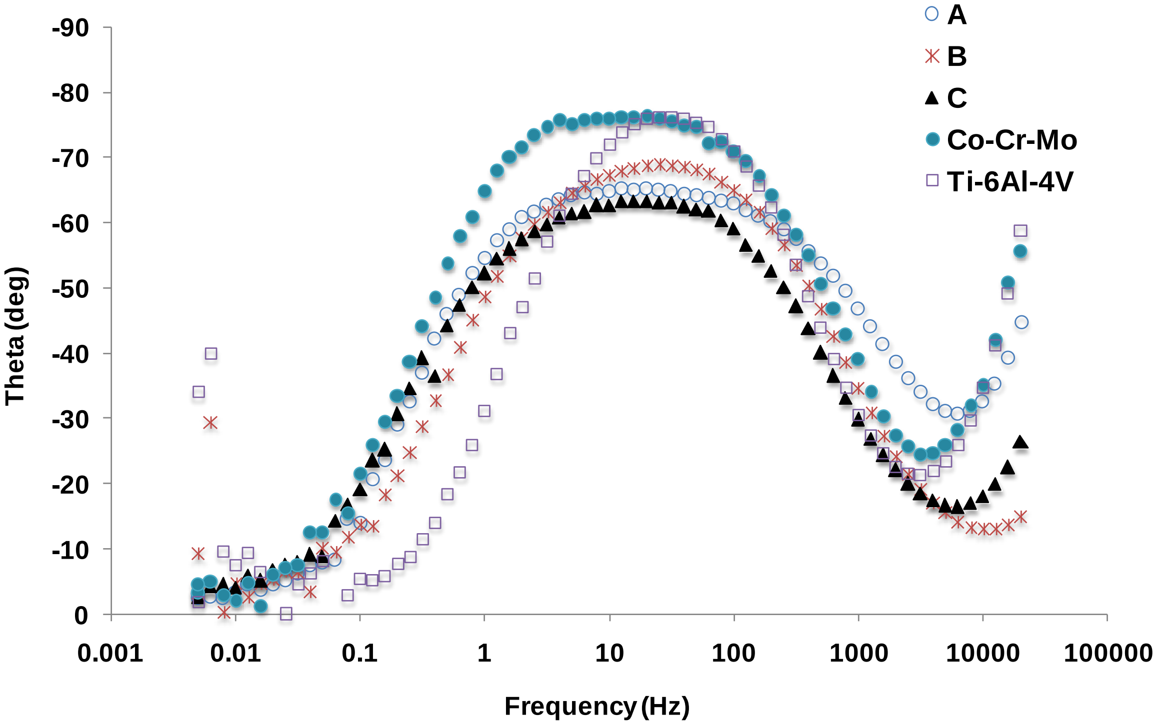

(b)

Figure 7: Bode plots for Cr-carbide coated and non-coated alloys exposed in the acidic high temperature H_2O_2 solution (pH 2) at the end of 1 hr immersion period. (a) Impedance plot (b) phase angle plot.

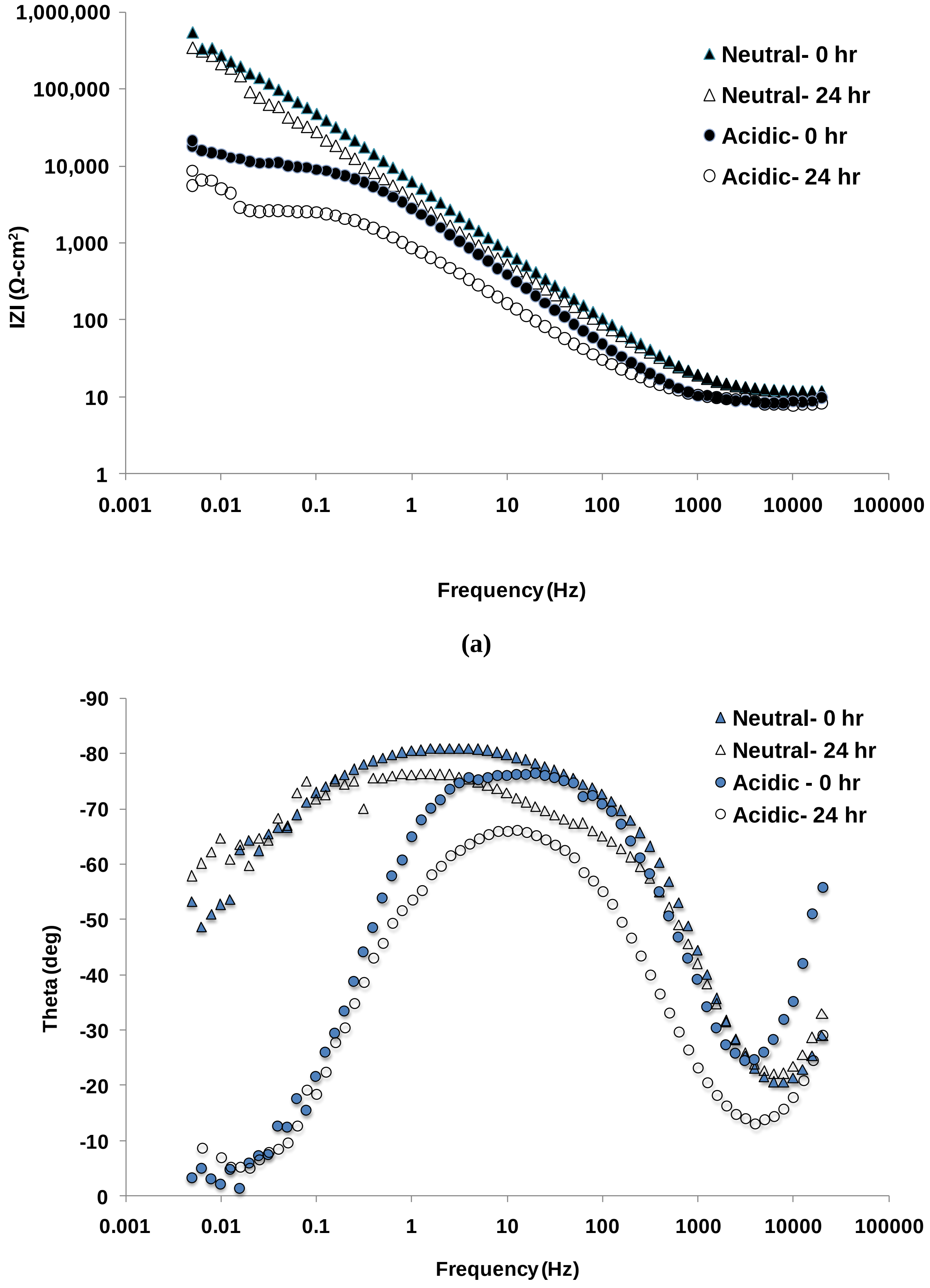

(a)

(b)

Figure 8: Bode plots for Co-Cr-Mo alloy exposed in neutral and acidic solution at different exposure times. (a) Impedance plot (b) Phase angle plot

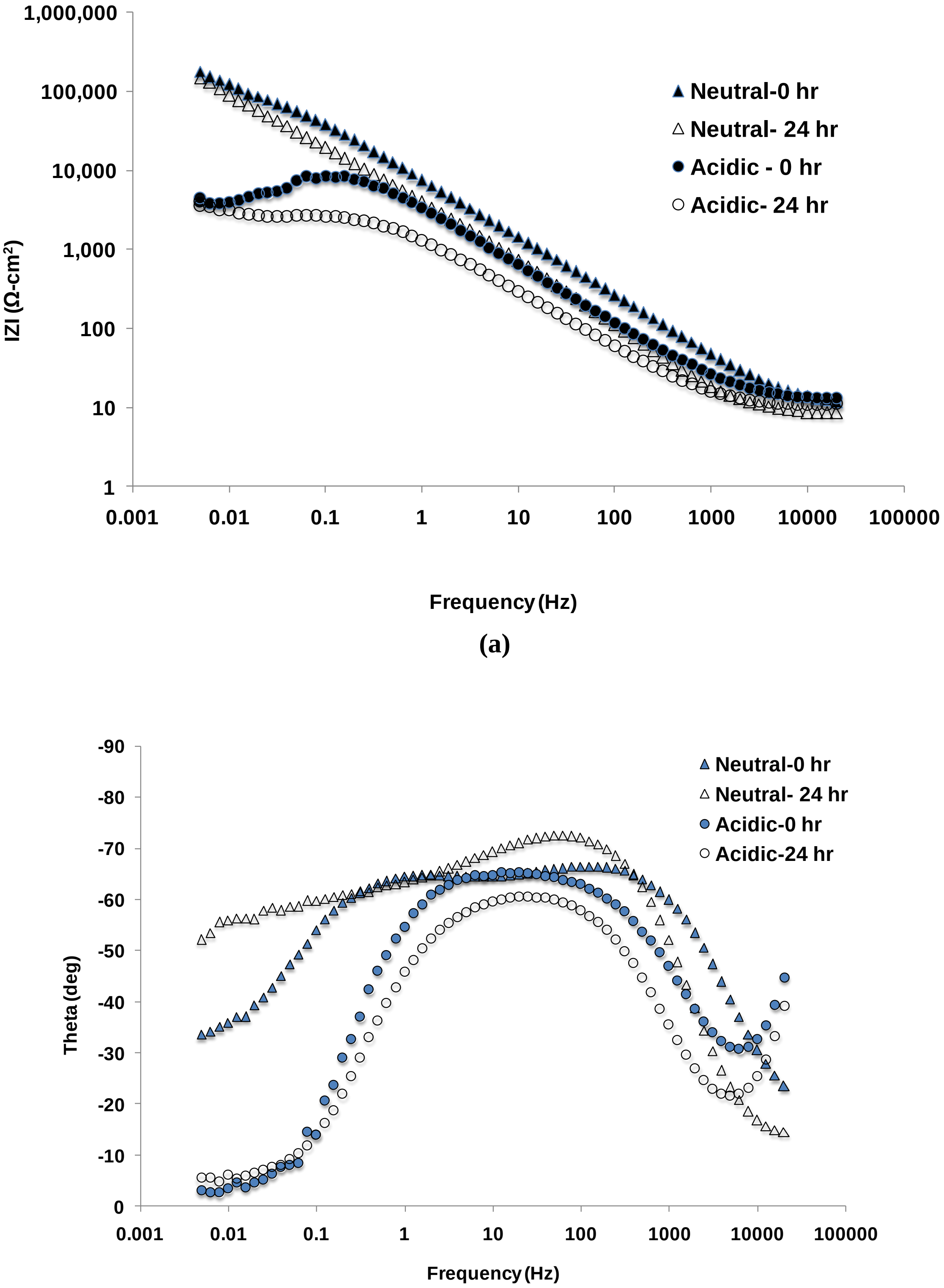

(a)

(b)

Figure 9: Bode plots for Cr-carbide coated (sample #A) exposed in neutral and acidic solution at different exposure times. (a) Impedance plot (b) Phase angle plot

Table 1: Overview of materials tested in this study

Materials	Deposition pressure conditions	Coating conditions	Diameter (mm)	Sample ID
Nanocarbide coating on Co-Cr-Mo	Atmospheric	Polished and gamma sterilized	40	#A
Nanocarbide coating on Ti-6Al-4V	Atmospheric	Polished and gamma sterilized	40	#B
Nanocarbide coating on Co-Cr-Mo	Atmospheric	Polished, passivated and gamma sterilized	40	#C
Ti-6Al-4V			42	Ti-6Al-4V
Co-Cr-Mo			42	Co-Cr-Mo

Table 2: Electrochemical parameters of the test samples: Open circuit potential (E_{ocp}) calculated at the end of 1hr under open circuit conditions, zero current potential (ZCP) calculated from polarization curves, transpassive potential (E_t) calculated from polarization curves at current density value of 10μA/cm^2, and corrosion current density (I_{corr}) derived from extrapolation of the cathodic portion of the polarization curve. (PBS, pH 7.4)

Sample	E_{OCP} V vs Ag/AgCl)	ZCP (V vs Ag/ AgCl)	E_t (V)	I_{corr} (μA/cm^2)
#A	-0.073 ± 0.075	-0.184 ± 0.028[a]	0.585 ± 0.002[a]	0.51 ± 0.169[ab]
#B	-0.090 ± 0.03	-0.282 ± 0.034[a]	0.545 ± 0.023[ac]	0.6 ± 0.036[ab]
#C	-0.016 ± 0.114	-0.491 ± 0.094[b]	0.198 ± 0.024[b]	4 ± 2.169[ab]
Ti-6Al-4V*	0.018 ± 0.099	-0.259 ± 0.032[a]	-----	0.25± 0.12[a]
Co-Cr-Mo*	-0.019 ± 0.006	-0.621 ± 0.106[b]	0.505 ± 0.012[c]	6 ± 4.17[b]

All values are denotes as mean ± SD for n=3

----- denotes no E_t value was available for Ti-6Al-4V

[a,b,c] represent significant differences between samples in terms of the parameter associated with each column.

* Data previously reported[10]

Table 3: Simulated impedance parameters found by nonlinear least square fitting of the electrical model circuits to the impedance data obtained for the neutral solution at 0 hour and 24 hour immersion time points.

Sample	R_s (Ω-cm^2)		CPE$_{coat}$ [(μF/cm^2)(rad/s)$^{1-\alpha}$], α		R_{coat} (Ω-cm^2)		CPE$_{ox}$ [(μF/cm^2)(rad/s)$^{1-\alpha}$], α		R_{ox} (MΩ-cm^2)	
	0 hr	24 hr	0 hr	24 hr	0 hr	24 hr	0 hr	24 hr	0 hr	24 hr
#A	15.86 ± 12.80	11.81 ± 4.35	28 ± 5, *0.8 ± 0.05*^{a}	39 ± 12, *0.82 ±0.09*^{a}	2177 ± 965	2963 ± 1864	20 ± 8, *0.68 ±0.14*	42 ± 13.2, *0.67 ± 0.12*	3.4 ± 5.62	3.7 ± 4.08
#B	17.48 ± 9.74	10.69 ± 8.45	26 ± 7 , *0.82 ± 0.04*$^{a, x}$	84 ± 40, *0.71±0.02*$^{ab, y}$	3895 ± 1691	1661 ± 887	31 ± 15, *0.57 ±0.14*	80 ± 45, *0.59 ± 0.26*	1 ± 0.5	0.95 ± 0.99
#C	10.24 ± 0.6	8.49 ± 1.21	158 ± 95 , *0.67 ± 0.06*^{b}	451 ± 319, *0.6 ± 0.07*^{b}	2464 ± 1532	383 ± 361	47 ± 50, *0.78 ± 0.2*	264 ± 370, *0.75 ± 0.19*	0.08 ±0.04	0.01 ± 0.01
Ti-6Al-4V	23.47 ± 23.63	23.39 ± 22.29	–	–	–	–	26 ± 4.23, *0.89 ± 0.01*	79 ± 55, *0.86 ± 0.07*	0.8 ± 0.17	1.7 ± 2.03
Co-Cr-Mo	20.51 ± 13.20	10.88 ± 0.36	–	–	–	–	25 ± 6.75, *0.92 ± 0.04*	35 ± 21, *0.89 ± 0.05*	0.3 ± 0.23	0.42 ± 0.22

All values are denoted as mean ± SD for n=3.

$^{a, b}$ represent significant differences between samples in terms of parameter associated with each column

$^{x, y}$ represent significant differences between 0 and 24 hr time point for that particular sample group.

Italics denote ‘α’ value.

Table 4: Simulated impedance parameters found by nonlinear least square fitting of the electrical model circuits to the impedance data obtained for the acidic solution at 0 hour and 24 hour immersion time points.

Sample	R_s (Ω-cm^2)		CPE_{ox} $[(\mu F/cm^2)(rad/s)^{1-\alpha}]$, α		R_{ox} (KΩ-cm^2)	
	0 hr	24 hr	0 hr	24 hr	0 hr	24 hr
#A	9.42 ± 1.09	9.52 ± 1.45	105 ± 63, *0.75 ± 0.06*^{ab}	286 ± 133, *0.64 ± 0.09*^{a}	7.66 ± 3.68	2.68 ± 0.86
#B	11.38 ± 2.57	8.01 ± 0.72	79 ± 49, *0.79 ± 0.07*^{ab}	192 ± 74, *0.7 ± 0.05*^{ab}	9.17 ± 6.61	10.46 ± 2.30
#C	11.20 ± 6.46	22.51 ± 21.41	72 ± 9 , *0.69 ± 0.14*^{a}	243 ± 193, *0.69 ± 0.01*^{ab}	8.63 ± 2.13	7.83± 8.31
Ti-6Al-4V	9.87 ± 1.63	7.93 ± 2.53	42 ± 24 , *0.91 ± 0.03*^{b}	692 ± 534 , *0.85 ± 0.06*^{bc}	4.4 ± 4	1.2 ± 0.56
Co-Cr-Mo	12.37 ± 6.4	8.69 ± 1.12	34 ± 27 , *0.91 ± 0.02*^{b}	94 ± 115, *0.88 ± 0.08*^{c}	20 ± 15.4	14 ± 10.2

All values are denoted as mean ± SD for n=3.

No significant differences were observed within each sample group tested at different time points.

$^{a, b, c}$ represent significant differences between samples in terms of the parameter associated with each column.

Italics denote ‘α’ value.